



# Facile synthesis of polyaniline nanostructures with effective electromagnetic interference shielding performance

Munan Qiu<sup>1</sup> · Yang Zhang<sup>1</sup> · Bianying Wen<sup>1</sup>

Received: 4 November 2017 / Accepted: 12 April 2018 / Published online: 16 April 2018  
© Springer Science+Business Media, LLC, part of Springer Nature 2018

## Abstract

Polyaniline (PANI) with different nanostructures has been synthesized through a simple chemical oxidation method without using any hard or soft templates. A correlation between structure, chemical construction, electrical conductivity, and electromagnetic shielding properties were extensively investigated. The obtained PANI nanostructures exhibit various morphologies by just simply changing the doping acids. The PANI doped with hydrochloric acid (denoted as PANI-HCl) and doped with camphorsulfonic acid (denoted as PANI-CSA) exhibit the “holothurian-like” morphology, while the PANI doped with phosphoric acid (denoted as PANI-H<sub>3</sub>PO<sub>4</sub>) presents the nanofiber structure. The “holothurian-like” structure showed larger diameters and length than the nanofibers. During the three samples, the PANI-CSA exhibits the highest electrical conductivity ( $1.28 \pm 0.17 \text{ S cm}^{-1}$ ) due to the large oxidation extent, crystallinity, and crystallite size. An excellent electromagnetic interference (EMI) shielding effectiveness (SE) as 20.7 dB of PANI-CSA was achieved with the thickness of only 0.35 mm. All these samples present an absorption-dominated shielding mechanism. Moreover, the SE values obtained from the experiments are higher than the theoretical calculations. All these above results indicated that the EMI shielding performance and dielectric permittivity were strongly affected by the microstructure and the chemical construction. We believe that this one-step procedure represents a promising protocol to control the nanostructures and properties of PANI for applications as advanced EMI shielding materials.

## 1 Introduction

With the rapid development of electronic equipment and the high device density, electronic equipment generates severe electromagnetic irradiation. The electromagnetic interference (EMI) is also harmful to human health. This novel sort of pollution provides a strong motivation for developing EMI shielding materials to ensure the proper functions of the electronic equipment and safety of human beings [1–6]. Compared with the conventional metal-based materials, intrinsically conducting polymers (ICPs) are new alternative candidates for EMI shielding applications because of their lightness, good processability and excellent environmental stability [7, 8]. Among these conducting polymers, polyaniline (PANI) has shown great potential for practical

applications due to its facile synthesis, acid-doping/base-dedoping chemistry, low cost, and design flexibility [9, 10]. For instance, the PANI films were successfully grown over three-dimensional hybrid carbon assemblage substrate and EMI SE of 21 dB could be obtained in the Ku band [11]. PANI was dispersed into insulative styrene acrylonitrile to endow the light weight composite EMI shielding properties [12]. The electromagnetic shielding properties for the PANI-coated bagasse fiber composite could be enhanced due to the improved conductivity and the core-shell architecture [4].

During these PANI-based materials, PANI with fine nanostructures presents a more unique and advanced properties. Great efforts have been devoted to regulate the nanostructure of PANI. For example, the  $\beta$ -naphthalene sulfonic acid was used as the soft template to control the growth of PANI. The morphologies of obtained PANI were changed from nanotubes to microspheres [13]. PANI nanofibers was fabricated without using any templates by the galvanostatic method [14]. Although considerable research has been accomplished, many available techniques have some inherent disadvantages that limit their widespread applications. Specific examples include the harsh reaction

✉ Yang Zhang  
zhyang@iccas.ac.cn

✉ Bianying Wen  
wenbianying@tsinghua.org.cn

<sup>1</sup> Department of Material Science and Engineering, Beijing Technology and Business University, Beijing 100048, China

conditions, requirement for multistep procedures and complicated instrumentation. Thus, facile and versatile strategies for the fabrication of PANI with fine nanostructures are much desired. Most recently, it was reported that PANI nanofibers exhibited high electrical conductivity due to their large aspect ratio [15]. It is believed that the formation of the electrically conductive network is affected by the nanostructure size of the material. Thus, the electrical property is strongly correlated with nanostructures of PANI. It is well documented that the improved conductivity will result in the enhanced EMI shielding performance [16]. As a consequence, we are intrigued by the opportunity to manufacture the PANI with fine nanostructures to obtain the superior EMI shielding materials and investigate their underlying EMI shielding mechanism.

In this research, we developed a template-free approach to synthesize the PANI with the controlled nanostructure. The effects of doping acid on electrical conductivity, EMI SE and dielectric properties were extensively studied. These results showed that the nanostructure of PANI plays an important role on the electrical properties which affect directly on the total shielding effectiveness. Moreover, the different mechanisms that contribute in the shielding efficiency was also discussed.

## 2 Experiment

### 2.1 Materials

Aniline (99% purity) and L(-)-camphorsulfonic acid (CSA) (98%) were purchased from J&K Chemicals. Hydrochloric acid (HCl) (36.0–38.0%), phosphoric acid ( $\text{H}_3\text{PO}_4$ ) (85%) and ammonium peroxydisulfate (APS) were obtained from Beijing Chemical Works. Aniline was purified through distillation under reduced pressure before use. The other products were used directly without purification.

### 2.2 Synthesis of PANI

The PANI was fabricated as the followings. The 1 M acid solution was firstly prepared. The solution was divided into two equal parts labelled solution A and solution B. The temperature of the above solution was adjusted to 0–5 °C by using of an ice bath. Aniline monomer was introduced into solution A and APS oxidant was similarly dissolved in solution B. The synthesis was achieved by the drop wise addition of solution B into the solution A. The finally ratio of APS-to-aniline molar ratio was equal to 1.05. The mixture was kept stirred at 0–5 °C for 3 h. Finally, the PANI precipitate was filtered and washed with distilled water and ethyl alcohol for several times. The resulting powder was dried in vacuum oven at 60 °C for 24 h. Three doping acids were used in this

study including  $\text{H}_3\text{PO}_4$ , HCl, and CSA. The PANI doped with  $\text{H}_3\text{PO}_4$  was denoted as PANI- $\text{H}_3\text{PO}_4$ , the same meaning for PANI-HCl and PANI-CSA.

### 2.3 Characterization

The morphology was studied by scanning electron microscope (SEM, FEI Quanta FEG 250). Before imaging, all the samples were coated with a thin layer of gold. The Fourier transformed infrared spectroscopy (FTIR) spectra in the range of 4000–400  $\text{cm}^{-1}$  were taken by NICOLET iZ10 spectrometer. The thermogravimetric (TG) analysis was recorded using a TA TGA Q5000 (TA Instruments, Delaware, USA) at a heating rate of 20 °C  $\text{min}^{-1}$  from room temperature to 800 °C under a continuous flow of nitrogen at 40  $\text{mL min}^{-1}$ . Electrical conductivity measurements were evaluated by Van der Pauw four-probe method [17] using a RTS-9 system (Four Probes Tech, Guangzhou, China). The electromagnetic property, relative complex permeability and the relative complex permittivity were measured from 8.2 to 12.4 GHz (X-band) using an Agilent E5071C vector network analyzer (VNA, Agilent E5071C). Two-port TRL calibration was performed at the beginning of each test sequence in order to reduce or remove errors [18]. For electromagnetic characterization and conductivity measurement, the materials with 0.35 mm thickness were molded by applied pressure of 20 MPa for 3 min. The samples for the relative complex permeability and the relative complex permittivity testing were prepared by first dispersing the PANI powder in the molten paraffin wax, and then the homogeneous mixture was molded into a rectangular holder with a height of 2.00 mm. The mass ratio of powder to paraffin was 40:60.

## 3 Results and discussion

### 3.1 Morphology

The SEM micrographs of the obtained PANI are shown in Fig. 1. Nanofibers were found in PANI- $\text{H}_3\text{PO}_4$  as depicted in Fig. 1a, while the primary morphology of PANI-HCl and PANI-CSA show the “holothurian-like” structure, as shown in Fig. 1b, c. Thus, the morphologies appear to be affected by the medium used in the polymerization process. Additionally, the “holothurian-like” structure showed larger diameters and length than the nanofibers. For example, the diameters of both PANI-HCl and PANI-CSA are around  $90 \pm 15$  nm, while the PANI- $\text{H}_3\text{PO}_4$  is of  $75 \pm 10$  nm. The average length of PANI-CSA is about 470 nm, which is longer than that of PANI-HCl around 330 nm.

It is well accepted that at the beginning of the reaction, aniline exists as cations in the acid media [19, 20]. The polymerization process was started by adding APS.

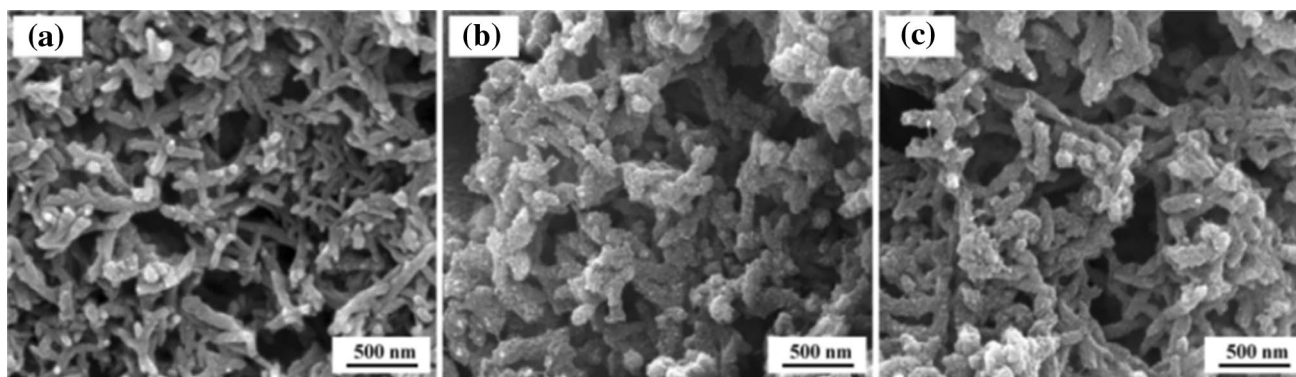


**Fig. 1** The typical SEM images of **a** PANI- $\text{H}_3\text{PO}_4$ , **b** PANI-HCl, **c** PANI-CSA

Then the formed oligomers ionized and reacted with other monomers or oligomers to produce PANI. Anilinium cations have both hydrophilic and lipophilic groups. The anilinium cations can form spherical micelles (represented by micelles A) in the solution before the oxidation. A part of aniline diffuses into micelles to form micelles B. The micelles A and B may serve as the templates for the formation of PANI nanostructures. Because the oxidant APS is water-soluble and can penetrate into the micelles, the reactions took place mainly at the micelle/water interface [21]. The micelles become big spheres through accretion or tubes/fibrils through elongation with the polymerization proceeding [22, 23]. Obviously, the elongation procedure dominates the growth of the PANI in this study. The nanostructures of the resulting PANI are directly related to the size of micelles. Hence, different morphologies could be obtained by adopting different acids.

In this research, aniline monomer is considered as molecular template for the growth of PANI nanofibers [24]. The formation of PANI chains is always followed by a rapid precipitation of the polymer. According to the classical nucleation (or precipitation) theory, the molecules need to accumulate to a specific supersaturation level first and then undergo nucleation and growth. The nuclei can be spontaneously (homogeneously) formed in the parent phase, or they can be heterogeneously grown on other species such as reactor surfaces or other particles in solution [25]. Therefore, we supposed that the  $\text{H}_3\text{PO}_4$  solution plays an important role in the connecting of the PANI particles leading to the self-assembled fibrous structure by suppressing secondary growth. On the other hand, the HCl and CSA solutions result in an increase in the granular particles over the fibers and “holothurian-like” structure can be obtained. The previous study also shows the morphology of PANI can be affected by the dopant, and the chemical structure of the doping acids could influence on the PANIs’ morphology [26–30].

### 3.2 FTIR spectroscopy

The FTIR spectra are depicted in the Fig. 2. It can be seen that similar spectra were exhibited for the obtained PANI. The band around  $3443\text{ cm}^{-1}$  corresponds to the N–H stretching vibration. The pair of bands near  $1578$  and  $1487\text{ cm}^{-1}$  are attributed to C=C stretching of quinonoid ( $\text{N}=\text{Q}=\text{N}$ ) and benzenoid ( $\text{N}=\text{B}=\text{N}$ ) rings, respectively [31, 32]. Moreover, C–N stretching of secondary aromatic amine is observed near  $1296\text{ cm}^{-1}$ , and the aromatic C–H in the quinoid ( $1130\text{ cm}^{-1}$ ) and benzene ( $795\text{ cm}^{-1}$ ) rings could be distinctly observed [33–35]. Besides, the absorption peaks in the O–H stretching deformations of doping acids could be found in  $2600\text{--}2900\text{ cm}^{-1}$ .

The characteristic peak of benzene ring was shift to  $1562$ ,  $1572\text{ cm}^{-1}$  for PANI-HCl and PANI-CSA, respectively. This indicates that in the backbone of PANI-HCl and PANI-CSA, the electron cloud density decreased and the vibration frequency reduced, resulting in more positive electron delocalized to the aromatic rings [36].

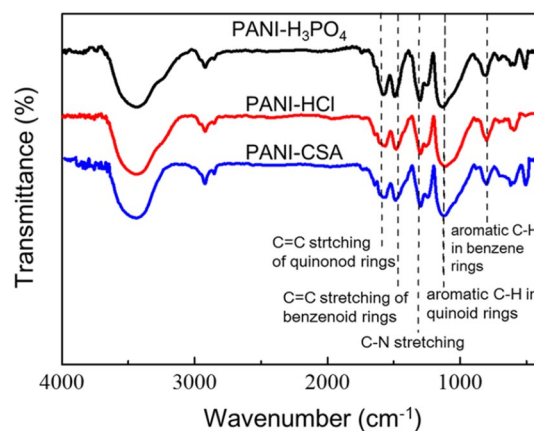


**Fig. 2** FTIR spectra of PANI doped with different acid

In general, the intensity ratio of absorption band of aromatic C–H of the quinoid ( $1130\text{ cm}^{-1}$ ) and the benzene ( $795\text{ cm}^{-1}$ ) rings represent the average extent of the oxidation state of the polymer, which reflects the content of the quinoid and benzene ring structures [37]:

$$R = I_{\text{quinoid}}/I_{\text{benzenoid}} \quad (1)$$

where  $R$  is the intensity ratio,  $I_{\text{quinoid}}$  and  $I_{\text{benzenoid}}$  is the intensity of the peak of aromatic C–H in quinoid ( $1130\text{ cm}^{-1}$ ) and benzene ( $795\text{ cm}^{-1}$ ) rings, respectively. It can be calculated from the spectrum that PANI-CSA exhibited the largest  $R$  (2.17), followed by PANI-HCl (1.97) and PANI-H<sub>3</sub>PO<sub>4</sub> (1.89). The different oxidation extent produces different doping densities [37]. It is well known that higher conductivity of PANI would be achieved with higher doping densities. Thus, it can be suggested that the different oxidation extent could further affect electrical properties of PANI.

### 3.3 X-ray diffraction analysis

It is well-known that the electrical conductivity of a conductive polymer depends on its crystallinity and the size of the crystal grains [17]. The peaks at  $2\theta$  angles of  $15.2^\circ$ ,  $20.1^\circ$  and  $25.2^\circ$  corresponding to (010), (100), and (110) plane reflections [15] are observed in Fig. 3. The peaks centered at  $20.1^\circ$  and  $25.2^\circ$  correspond to the periodicities parallel and perpendicular to the polymer chain, respectively. The peak at  $2\theta$  of  $25.2^\circ$  indicates the formation of doped PANI, since this peak is the characteristic of highly doped emeraldine salt of PANI [38].

The XRD patterns of the crystalline structures can be used to estimate the average crystallite size, lattice plane  $d$ -spacing, and crystallinity. The average crystallite size of PANI can be estimated using Scherrer formula [17].

$$D = 0.9\lambda/\beta \cos \theta \quad (2)$$

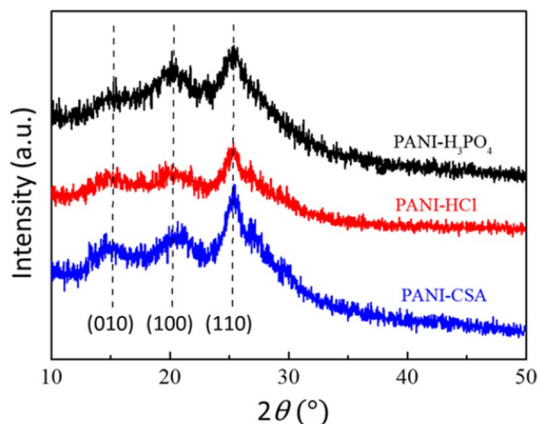


Fig. 3 X-ray diffraction patterns of doped-PANI

where  $D$  is the crystallite size,  $\lambda$  is wavelength of incident wave ( $1.5406\text{ \AA}$  for Cu K $\alpha$ ),  $\beta$  is full width at half maximum (FWHM) of the diffraction peak, and  $\theta$  is the Bragg diffraction angle.

The lattice space is calculated based on the Bragg's equation [39]:

$$n\lambda = 2d \sin \theta \quad (3)$$

where  $n$  is an integer (usually  $n = 1$ ),  $\lambda$  is the wavelength, and  $d$  is the spacing between the planes in the atomic lattice.

The lattice space and average crystallite size at (110) plane and crystallinity of samples are summarized in Table 1. There was no obvious difference in the lattice space, while the average crystallite size and the crystallinity significantly changes with the doping acid. From Eq. 3, it would be found that the lattice space is only associated with the diffraction angle  $2\theta$ . The (110) planes of all samples are located at almost the same  $2\theta$  value without any obvious peak shift. As can be seen from Table 1, PANI-CSA has the largest crystallite size among the samples, which followed by PANI-HCl, and PANI-H<sub>3</sub>PO<sub>4</sub> is with the smallest crystallite size. Crystallite size is decided by the diffraction angle and the FWHM. A narrow peak indicates a smaller FWHM and an increased crystallite size. Compared with PANI-H<sub>3</sub>PO<sub>4</sub> and PANI-HCl, a sharp and narrow peak of (110) plane is observed of PANI-CSA (Fig. 3). Thus, the crystallite size of the PANI-CSA is higher than other two samples.

### 3.4 Electrical conductivity

Figure 4 shows the conductivity of PANI-HCl, PANI-H<sub>3</sub>PO<sub>4</sub>, and PANI-CSA. The PANI-H<sub>3</sub>PO<sub>4</sub> displayed the lowest conductivity of  $0.84 \pm 0.10\text{ S cm}^{-1}$ . PANI-HCl and PANI-CSA possess electrical conductivities of  $1.22 \pm 0.16$  and  $1.28 \pm 0.17\text{ S cm}^{-1}$ , respectively. It is well accepted that the conductivity of PANI is mainly influenced by the chemical construction and crystal properties. The hydroxyl in the PANI-CSA generated the electron repulsion effect, which increased the conjugative effect in the PANI backbone and improved the conductivity. Meanwhile, the large crystal grain result in higher electrical conductivity [17]. The change in conductivity

Table 1 Diffraction angle, FWHM, lattice spacing, the average crystallite size of (110) lattice plane and crystallinity of PANI-H<sub>3</sub>PO<sub>4</sub>, PANI-HCl, and PANI-CSA

Designation	PANI-H <sub>3</sub> PO <sub>4</sub>	PANI-HCl	PANI-CSA
$2\theta$ ( $^\circ$ )	25.18	25.12	25.19
FWHM ( $^\circ$ )	1.80	1.34	1.29
Lattice spacing ( $d$ ) ( $\text{\AA}$ )	3.53	3.54	3.53
Crystallite size ( $D$ ) ( $\text{\AA}$ )	44.15	59.29	61.61
Crystallinity (%)	17.24	19.74	20.87

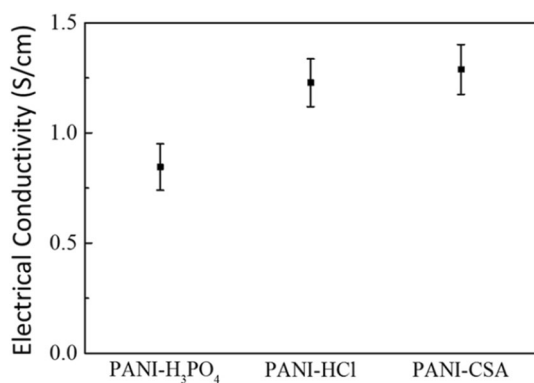


Fig. 4 The effect of doping acid on the conductivity of PANI

is consistent with FTIR and XRD results. Moreover, the protrusions on the fibers surface of PANI-CSA and PANI-HCl promote electron transfer between the adjacent fibers, which also increase the electrical conductivity.

### 3.5 EMI shielding effectiveness

EMI SE is the measurement of shielding against the penetration of electromagnetic radiation into a material. It can be defined as follows [4]:

$$SE = 10 \log(P_I/P_T) \tag{4}$$

It is evident that for a lossless material:

$$P_I = P_R + P_T + P_A \tag{5}$$

where  $P_T$  is the power of transmitted wave and  $P_I$  is the power of incident wave (1 mW),  $P_R$  is the reflected power density at same measuring point,  $P_A$  is the absorbed power [40, 41].

The SE value and the conductivity are related in the form:

$$SE = 20 \log(1 + \sigma d Z_0 / 2) \tag{6}$$

where  $\sigma$  is the conductivity ( $S\text{ cm}^{-1}$ ) of the sample,  $d$  is the thickness, and  $Z_0$  is the free-space wave impedance (377 ohm).

The overall EMI SE in the X-band of PANI-HCl, PANI- $H_3PO_4$  and PANI-CSA are illustrated in Fig. 5. The SE values for PANI-HCl and PANI-CSA are about 20.7 dB, while the SE for PANI- $H_3PO_4$  is about 17.1 dB. This result is consistent with the general rule that the SE is proportional to the material conductivity, as illuminate in Eq. (6).

In order to clarify the EMI shielding mechanism, net shielding by reflection loss ( $SE_R$ ) and absorption loss ( $SE_A$ ) were calculated using the power balance data. Equations (7) and (8) are the mathematical interpretation of definitions [16].

$$SE_R = 10 \log \frac{P_I}{1 - P_R} \tag{7}$$

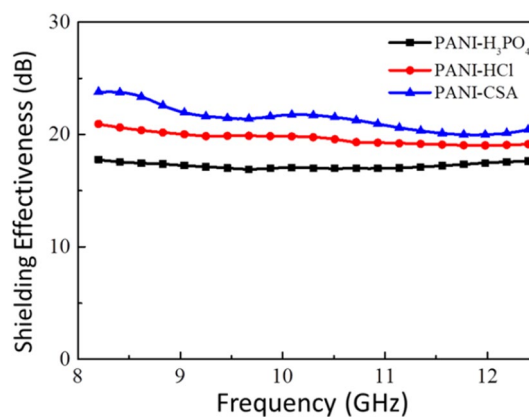


Fig. 5 EMI SE as a function of frequency for the PANI- $H_3PO_4$ , PANI-HCl, and PANI-CSA

$$SE_A = 10 \log \frac{1 - P_R}{P_T} \tag{8}$$

Moreover, a theoretical analysis is conducted for further understand the electromagnetic shielding mechanism. Equations (9) and (10) are developed to quantify the contribution of reflection and absorption to the overall EMI SE.

$$SE_R = 39.5 + 10 \log \frac{\sigma}{2\pi f \mu} \tag{9}$$

$$SE_A = 8.7d\sqrt{\pi f \mu \sigma} \tag{10}$$

where  $\mu$  is the material’s magnetic permeability ( $\mu = \mu_0 \mu_r$ ),  $\mu_0 = 4\pi \times 10^{-7} \text{ H m}^{-1}$ ,  $\mu_r$  is the material’s relative magnetic permeability [42].

Table 2 presents a comparison between the experimental results and the theoretical prediction of the doped-PANI at the frequency of 10 GHz. It was observed that the values of  $SE_A$  were larger than  $SE_R$  for both experimental and theoretical results. Therefore, the obtained PANI presents a shielding effectiveness by absorption mechanism. In addition, the experimental values of the overall EMI SE,  $SE_A$ , and  $SE_R$  are much larger than the theoretical predictions for all the samples. The difference between experimental and theoretical results may be attributed to the facts that assumptions taken in derivation of used simplified equations and the theoretical model ignores the multiple-reflection effect. From the above discussion, it could be deduced that for such type of PANI with fine nanostructure, the complex internal surface reflection and/or absorption of electromagnetic wave were induced by their unique nanostructure. The multiple-reflection effect was increased significantly by the complex fine structure. Thus, the total EMI SE enhanced compared to the theoretical predictions.

**Table 2** Comparison between EMI SE data experimentally obtained and theoretically calculated for the doped-PANI (10 GHz)

Designation	Electrical conductivity ( $S\text{ cm}^{-1}$ )	$SE_{\text{Total}}$ (dB)		$SE_{\text{A}}$ (dB)		$SE_{\text{R}}$ (dB)	
		Exp.	Theory	Exp.	Theory	Exp.	Theory
PANI- $H_3PO_4$	$0.84 \pm 0.10$	17.05	6.91	12.31	5.56	4.73	1.35
PANI-HCl	$1.22 \pm 0.16$	19.83	9.67	14.89	6.70	4.94	2.97
PANI-CSA	$1.28 \pm 0.17$	20.71	10.04	14.74	6.86	5.97	3.18

### 3.6 Dielectrical and magnetic properties

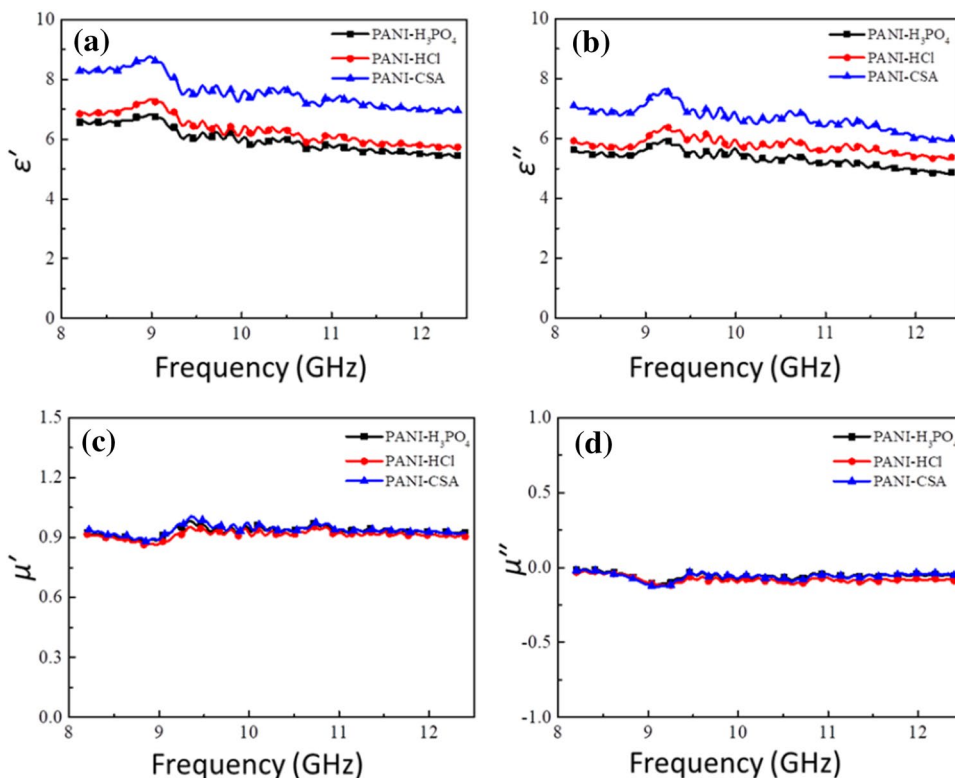
Apart from electrical conductivity, the relative complex permittivity and permeability are also important factors in determining electromagnetic properties. The complex dielectric constant can be separated into its real part ( $\epsilon'$ ) and imaginary part ( $\epsilon''$ ).  $\epsilon'$  is known as dielectric constant or relative permittivity, while  $\epsilon''$  is known as loss factor or dielectric loss. The complex permittivity  $\epsilon_r$  ( $\epsilon_r = \epsilon' - j\epsilon''$ ) of the doped-PANI are shown in Fig. 6a, b. The  $\epsilon'$  values is same with the law of conductivity. The high permittivity reflects the high electric flux in materials due to the enhanced polarization of electron clouds. In this study, the highest permittivity was detected in the PANI-CSA. This result is similar with the previous studie [41, 43].

Figure 6c, d shows the real part ( $\mu'$ ) and the imaginary part ( $\mu''$ ) of the permeability of the samples. The value of  $\mu'$  and  $\mu''$  represent the capability for magnetic energy storage and loss, respectively. The values of  $\mu'$  and  $\mu''$  for all the samples are around 1 and 0, respectively. Both  $\mu'$  and  $\mu''$

exhibit relatively low values for all of the samples compared with the  $\epsilon'$  and  $\epsilon''$ . This indicates that all obtained PANI is non-magnetic material. Thus the main contribution of the microwave loss should come from their dielectric loss [41].

### 4 Conclusions

The acid doped-PANIs with effective EMI shielding ability were synthesized by a simple chemical oxidation strategy. The doping acids with different polarities lead to the self-assembly of PANI particles into fine nanostructures by inhibiting secondary growth. The PANI- $H_3PO_4$  shows the nanofibers morphology, while the PANI-HCl and PANI-CSA present the “holothurian-like” structure. The results indicated that morphology and chemical constitution of PANI would be controlled by doping acid, which would further affect on the electrical and the EMI shielding properties. Moreover, the absorption is dominated to the total EMI SE of 20.7 dB for PANI-CSA at a thickness of 0.35 mm

**Fig. 6** The real **a** and the imaginary **b** part of permittivity of doped-PANI, the real **c** and the imaginary **d** part of permeability of doped-PANI

suggests the usefulness of the material for electromagnetic shielding. The main contribution of the microwave loss comes from the dielectric loss.

**Acknowledgements** This work was financially supported by the National Natural Science Foundation of China (21274007), Young Core Personal Project & Beijing Outstanding Talent Training Project (2017000020124G079), the Science and Technology Development Project of Beijing Municipal Commission of Education (SQKM201610011001), Innovative Research Team of Polymeric Functional Film of Beijing Technology and Business University (19008001071), the Two Sections Cultivation Fund of Beijing Technology and Business University (LKJJ2016-23), and Beijing College Students' Scientific Research Training Program.

## References

1. A.N. Esfahani, A.A. Katbab, A. Taeb, L. Simon, M.A. Pope, Correlation between mechanical dissipation and improved X-band electromagnetic shielding capabilities of amine functionalized graphene/thermoplastic polyurethane composites. *Eur. Polym. J.* **95**, 520–538 (2017)
2. Y. Zhang, X. Fang, B. Wen, W. Zou, Facile preparation of asymmetric Ni/PVC film with controlled structure: application as a high-performance EMI shielding material. *J. Appl. Polym. Sci.* **132**, 42560 (2015)
3. Z. Durmus, A. Durmus, M.Y. Bektay, H. Kavas, I.S. Unver, B. Aktas, Quantifying structural and electromagnetic interference (EMI) shielding properties of thermoplastic polyurethane-carbon nanofiber/magnetite nanocomposites. *J. Mater. Sci.* **51**, 8005–8017 (2016)
4. Y. Zhang, M. Qiu, Y. Yu, B. Wen, L. Cheng, A novel polyaniline-coated bagasse fiber composite with core-shell heterostructure provides effective electromagnetic shielding performance. *ACS Appl. Mat. Interfaces* **9**, 809–818 (2017)
5. B.G. Soares, N. Riany, A.A. Silva, G.M.O. Barra, S. Livi, Dual-role of phosphonium: based ionic liquid in epoxy/MWCNT systems: electric, rheological behavior and electromagnetic interference shielding effectiveness. *Eur. Polym. J.* **84**, 77–88 (2016)
6. Y. Zhang, X.X. Fang, B.Y. Wen, Asymmetric Ni/PVC films for high-performance electromagnetic interference shielding. *Chin. J. Polym. Sci.* **33**, 899–907 (2015)
7. B. Altava, V. Compañ, A. Andrio, L. del Castillo, S. Mollá, M. Burguete, E. Garcia-Verdugo, S. Luis, Conductive films based on composite polymers containing ionic liquids absorbed on crosslinked polymeric ionic-like liquids (SILLPs). *Polymer* **72**, 69–81 (2015)
8. B. Somboonsub, S. Srisuwan, M.A. Invernale, S. Thongyai, P. Praserttham, D.A. Scola, G.A. Sotzing, Comparison of the thermally stable conducting polymers PEDOT, PANi, and PPy using sulfonated poly (imide) templates. *Polymer* **51**, 4472–4476 (2010)
9. G. Ćirić-Marjanović, Recent advances in polyaniline research: polymerization mechanisms, structural aspects, properties and applications. *Synth. Met.* **177**, 1–47 (2013)
10. S. Srisuwan, S. Thongyai, G.A. Sotzing, P. Praserttham, Preparation and characterization of conductive polyimide-graft-polyaniline. *Microelectron. Eng.* **104**, 22–28 (2013)
11. A.K. Sharma, P. Bhardwaj, K.K. Singh, S.K. Dhawan, Improved microwave shielding properties of polyaniline grown over three-dimensional hybrid carbon assemblage substrate. *Appl. Nanosci.* **5**, 635–644 (2015)
12. A. Saboor, A.N. Khan, H.M. Cheema, K. Yaqoob, A. Shafqat, Effect of polyaniline on the dielectric and EMI shielding behaviors of styrene acrylonitrile. *J. Mater. Sci.: Mater. Electron.* **27**, 9634–9641 (2016)
13. N.P. Tavandashti, M. Ghorbani, A. Shojaei, Controlled growth of hollow polyaniline structures: from nanotubes to microspheres. *Comput. Theor. Polym. Sci.* **54**, 5586–5594 (2013)
14. E.M. Erro, A.M. Baruzzi, R.A. Iglesias, Fast electrochromic response of ultraporous polyaniline nanofibers. *Polymer* **55**, 2440–2444 (2014)
15. X. Zhang, J. Zhu, N. Haldolaarachchige, J. Ryu, D.P. Young, S. Wei, Z. Guo, Synthetic process engineered polyaniline nanostructures with tunable morphology and physical properties. *Polymer* **53**, 2109–2120 (2012)
16. L.C. Jia, D.X. Yan, C.H. Cui, X. Jiang, X. Ji, Z.M. Li, Electrically conductive and electromagnetic interference shielding of polyethylene composites with devisable carbon nanotube networks. *J. Mater. Chem. C* **3**, 9369–9378 (2015)
17. T. David, J.K. Mathad, T. Padmavathi, A. Vanaja, Synthesis of polyaniline and carboxylic acid functionalized SWCNT composites for electromagnetic interference shielding coatings. *Polymer* **55**, 5665–5672 (2014)
18. A.R.A. Schettini, D. Khastgir, B.G. Soares, Microwave dielectric properties and EMI shielding effectiveness of poly(styrene-*b*-styrene-butadiene-*b*-styrene) copolymer filled with PANi. Dodecylbenzenesulfonic acid and carbon black. *Polym. Eng. Sci.* **52**, 2041–2048 (2012)
19. T. Anwer, M.O. Ansari, F. Mohammad, Dodecylbenzenesulfonic acid micelles assisted in situ preparation and enhanced thermoelectric performance of semiconducting polyaniline-zirconium oxide nanocomposites. *J. Ind. Eng. Chem.* **19**, 1653–1658 (2013)
20. N.R. Chiou, L.J. Lee., A.J. Epstein, Self-assembled polyaniline nanofibers/nanotubes. *Chem. Mater.* **19**, 3589–3591 (2007)
21. L.J. Zhang, M.X. Wan, Synthesis and characterization of self-assembled polyaniline nanotubes doped with D-10-camphorsulfonic acid. *Nanotechnology* **13**, 750–755 (2002)
22. G.H. Lim, H.J. Choi, Synthesis of self-assembled rectangular-shaped polyaniline nanotubes and their physical characteristics. *J. Ind. Eng. Chem.* **47**, 51–55 (2017)
23. J. Stejskal, I. Sapurina, M. Trchová, Polyaniline nanostructures and the role of aniline oligomers in their formation. *Prog. Polym. Sci.* **35**, 1420–1481 (2010)
24. D. Li, R.B. Kaner, Shape and aggregation control of nanoparticles: not shaken, not stirred. *J. Am. Chem. Soc.* **128**, 968–975 (2006)
25. N. Joseph, J. Varghese, M. Sebastian, Self assembled polyaniline nanofibers with enhanced electromagnetic shielding properties. *RSC Adv.* **5**, 20459–20466 (2015)
26. Z. Zhang, Z. Wei, L. Zhang, M. Wan, Polyaniline nanotubes and their dendrites doped with different naphthalene sulfonic acids. *Acta Mater.* **53**, 1373–1379 (2005)
27. F.X. Perrin, T.A. Phan, D.L. Nguyen, Preparation and characterization of polyaniline in reversed micelles of decylphosphonic acid for active corrosion protection coatings. *Eur. Polym. J.* **66**, 253–265 (2015)
28. A. Drelinkiewicz, Z. Kalemba-Jaje, E. Lalik, R. Kosydar, Organosulfonic acids doped polyaniline: based solid acid catalysts for the formation of bio-esters in transesterification and esterification reactions. *Fuel* **116**, 760–771 (2014)
29. J. Wang, K. Zhang, L. Zhao, Sono-assisted synthesis of nanostructured polyaniline for adsorption of aqueous Cr(VI): effect of protonic acids. *Chem. Eng. J.* **239**, 123–131 (2014)
30. M. Bláha, M. Varga, J. Prokeš, A. Zhigunov, J. Vohlřídál, Effects of the polymerization temperature on the structure, morphology and conductivity of polyaniline prepared with ammonium peroxodisulfate. *Eur. Polym. J.* **49**, 3904–3911 (2013)
31. F. Rezaei, N.P. Tavandashti, A.R. Zahedi, Morphology of polyaniline nanofibers synthesized under different conditions. *Res. Chem. Intermed.* **40**, 1233–1247 (2014)

32. A.M. Youssef, Morphological studies of polyaniline nanocomposite based mesostructured TiO<sub>2</sub> nanowires as conductive packaging materials. *RSC Adv.* **4**, 6811–6820 (2013)
33. S. Atifi, W.Y. Hamad, Emulsion-polymerized flexible semi-conducting CNCs–PANI–DBSA nanocomposite films. *RSC Adv.* **6**, 65494–65503 (2016)
34. O. Abdulrazzaq, S.E. Bourdo, V. Saini, F. Watanabe, B. Barnes, A. Ghosh, A.S. Biris, Tuning the work function of polyaniline via camphorsulfonic acid: an X-ray photoelectron spectroscopy investigation. *RSC Adv.* **5**, 33–40 (2014)
35. S. Tao, B. Hong, Z. Kerong, An infrared and Raman spectroscopic study of polyanilines co-doped with metal ions and H<sup>+</sup>. *Spectrochim. Acta A* **66**, 1364–1368 (2007)
36. H.R. Tantawy, D.E. Aston, J.R. Smith, J.L. Young, Comparison of electromagnetic shielding with polyaniline nanopowders produced in solvent-limited conditions. *ACS Appl. Mater. Interfaces* **5**, 4648–4658 (2013)
37. N. Joseph, J. Varghese, M.T. Sebastian, Self assembled polyaniline nanofibers with enhanced electromagnetic shielding properties. *RSC Adv.* **5**, 20459–20466 (2015)
38. M. Das, D. Sarkar, Effect of oxidizing agent on ammonia sensing of DBSA doped polyaniline nanocomposite thin film. *J. Mater. Sci.: Mater. Electron.* **27**, 4109–4119 (2016)
39. M. Magioli, B.G. Soares, A.S. Sirqueira, M. Rahaman, D. Khastgir, EMI shielding effectiveness and dielectrical properties of SBS/PAni.DBSA blends: effect of blend preparation. *J. Appl. Polym. Sci.* **125**, 1476–1485 (2012)
40. A.R.A. Schettini, B.G. Soares, Study of microwave absorbing properties of polyaniline/STF conducting composites prepared by in situ polymerization. *Macromol. Symp.* (2011). <https://doi.org/10.1002/masy.200900106>
41. M.H. Al-Saleh, U. Sundararaj, Electromagnetic interference shielding mechanisms of CNT/polymer composites. *Carbon* **47**, 1738–1746 (2009)
42. Y. Chen, Y. Li, M. Yip, N. Tai, Electromagnetic interference shielding efficiency of polyaniline composites filled with graphene decorated with metallic nanoparticles. *Compos. Sci. Technol.* **80**, 80–86 (2013)
43. H. Ghasemi, U. Sundararaj, Electrical properties of in situ polymerized polystyrene/polyaniline composites: the effect of feeding ratio. *Synth. Met.* **162**, 1177–1183 (2012)